1-D FEM-Based Approach for Extracting Dimension-Independent Material Properties of Mn-Zn Toroidal Ferrite Cores

Reda Elkhadrawy, Jay Panchal, Timo Tarhasaari, Kari Lahti, and Paavo Rasilo

Electrical Engineering Unit, Tampere University, 33720 Tampere, Finland

This article presents a finite element (FE) method (FEM)-based approach for identifying the dimension-independent magnetic and dielectric properties of Mn-Zn toroidal ferrite cores. Two 1-D axisymmetric FE models are used for solving the full-wave electromagnetic field equations in a toroidal ferrite core using either the electric field strength (E) or the magnetic field strength (H) as the variable. Impedance measurements are performed for the toroidal cores over a frequency range of 10 kHz–10 MHz. The FE models and the impedance measurements are combined with a non-linear least-squares algorithm for solving the inverse problem for extracting the dimension-independent values of complex permeability and complex permittivity. The extracted permeability is validated against the datasheet of the measured samples.

Index Terms— **Complex permeability, complex permittivity, dimensional resonance, ferrites, finite element method, inverse problem.**

I. Introduction

MANGANESE-ZINC ferrites have been extensively used in high-frequency electromagnetic devices because of their low energy losses [1]. Still, the loss mechanisms in ferrites have not been fully revealed, mainly due to the lack of knowledge about their intrinsic magnetic and electrical properties. Although the permeability is usually the main parameter for designing ferrite cores, the complex permittivity plays a big role in core losses, especially when the operating frequency is in the MHz range [2]. Thus, complex permittivity should be considered during the design of high-frequency power electronic devices based on ferrite cores.

Ferrite suppliers do not usually provide any information about the conductivity and permittivity of ferrite cores. Therefore, modeling and measuring ferrite cores have been popular research topics in the past few decades. Due to the combination of high permeability and high permittivity, ferrite cores are subject to dimensional resonance effects at high frequency. The cause of such effects is the occurrence of standing electromagnetic waves whose wavelength is of the same order of magnitude as the size of the core [3]. Because of these dimensional effects, direct measurement of the dimension-independent or "intrinsic" material properties is a difficult task. Thus, inverse approaches need to be developed for extracting the intrinsic parameters based on measurements.

A common approach for modeling ferrite cores is based on solving the wave equation for the electric and/or the magnetic field in the ferrite core and extracting the dimension-independent complex permeability $\mu_{\text{core}} = (\mu_{\text{r}}' - j\mu_{\text{r}}'')\mu_0$ and complex permittivity $\varepsilon_{\text{core}} = (\varepsilon_{\text{r}}' - j\varepsilon_{\text{r}}'')\varepsilon_0$ by fitting the calculated impedance to the measured values [4]–[7]. Huang and Zhang proposed an approach which is based on solving analytically the electric field in a cuboid ferrite capacitor [5]. The impedance measurements and the analytical model were combined with the Newton–Raphson method to identify the dimension-independent values of μ_{core} and $\varepsilon_{\text{core}}$ of the samples. Stadler *et al.* proposed a methodology similar to Huang's work for measuring the AC conductivity and the dielectric constant of Mn-Zn toroidal ferrite cores at different temperatures [7]. However, it was not clear how μ_{core} is considered in the inverse approach presented in [7]. Another drawback of the previous models is that only one of the extracted parameters, i.e., either μ_{core} or $\varepsilon_{\text{core}}$, is validated against the magnetic or dielectric measurements used in the inverse algorithm, respectively.

The main objective of this work is to develop a finite element (FE) method (FEM)-based approach for extracting the dimension-independent electromagnetic material parameters, i.e., μ_{core} and $\varepsilon_{\text{core}}$ of toroidal Mn-Zn ferrite cores and address the aforementioned drawbacks. The extracted μ_{core} and $\varepsilon_{\text{core}}$ are validated against the supplier datasheet and dielectric measurements carried out by the authors, respectively. The measurement setup and the impedance measurements for the toroidal samples are discussed first in Section II, and the computational models are derived later in the same section. The fitting results and the extracted dimension-independent electromagnetic parameters are presented in Section III. Section IV is devoted to discussion and conclusion.

II. Methods

A. Impedance Measurements

Impedance measurements for three toroidal cores are carried out at room temperature in the frequency range of 10 kHz–10 MHz with Novocontrol Alpha-A Modular dielectric/impedance measurement system in combination with ZG4 extension test interface and standard sample cell BDS1200 [8]. The measurement setup has a frequency limitation of 10 MHz, and the sample cell has height and diameter limitations of 15 and 40 mm, respectively. The sample is placed between

Manuscript received 9 February 2022; revised 6 June 2022; accepted 27 June 2022. Date of publication 4 July 2022; date of current version 26 August 2022. Corresponding author: R. Elkhadrawy (e-mail: reda.elkhadrawy@tuni.fi).

Color versions of one or more figures in this article are available at https://doi.org/10.1109/TMAG.2022.3187539.

Digital Object Identifier 10.1109/TMAG.2022.3187539

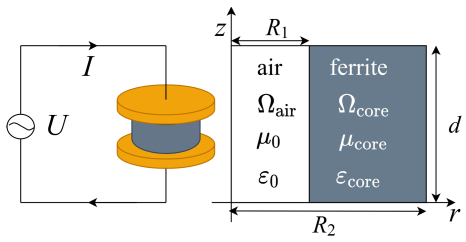

Fig. 1. Electrical circuit representation of impedance measurements for the ferrite samples (left) and the geometry of the cross section (toroidal core+air) under study (right).

TABLE I
DATA AND DIMENSIONS OF THE SAMPLES

Sample name	T22/14/6	T26/16/8	T36/23/10
Material group	F-material	F-material	F-material
μ'_r at 10 kHz	$3000 \pm 20\%$	$3000 \pm 20\%$	$3000 \pm 20\%$
Country of origin	China	Poland	USA
Lot number	CF20MK218	P01640	59669-1
Serial number	0F42206TC	0F42507TC	0F43610TC
$2R_2$ (mm)	22.2	25.6	36.2
$2R_1$ (mm)	13.7	15.6	23.2
d (mm)	6.39	7.95	10
σ_{DC} (S/m)	0.124	0.087	0.385

two electrodes, a sinusoidal voltage is imposed across the sample, and the total current through the sample is measured according to Fig. 1 (left). The samples were provided by Magnetics®, and their data are shown in Table I [9]. To get rid of the contact resistance, the top and bottom surfaces of the samples were coated with two layers of nickel and gold of thicknesses of 0.01 and 0.1 μm, respectively, using an electron beam evaporation setup. Moreover, before carrying out any measurements for each core, open-circuit, short-circuit, and standard load calibrations of the measurement setup were performed to minimize the measurement errors.

If ferrite cores have the same chemical composition and preparation process, it is reasonable to assume that they share the same intrinsic material properties, at least with an accuracy related to the repeatability of the manufacturing process. According to the equivalent circuit approach which models the ferrite core using constant phase elements [10], [11], the phase angles of samples with identical material properties should be equal until the occurrence of the dimensional resonance. From the phase angles of the measured samples shown in Fig. 2, it is clear that the samples do not share exactly the same material properties. Even if all the samples were in the same delivery and, according to the supplier, they belong to the same F-material category with initial permeability $\mu'_r = 3000 \pm 20\%$ at 10 kHz, we can see from the data in Table I that the samples do not come from the same lot and do not even have the same country of origin. If the samples are excited by electric field, the phase angle first decreases when the frequency increases, since the samples behave as imperfect capacitors. However, the significance of the magnetic field increases with frequency, and it can be noticed from Fig. 2 that the phase angle changes direction at some point, e.g., at about 250 kHz for T36/23/10. The dimensional resonance behavior

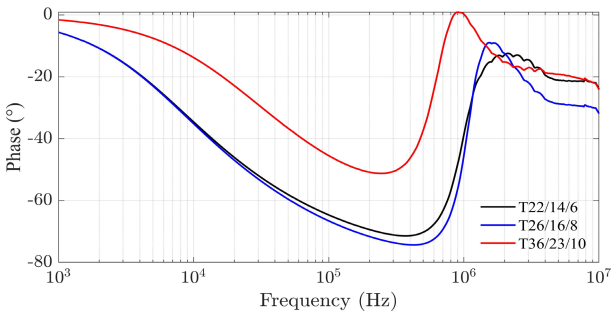

Fig. 2. Phase angle of the measured impedances for the Mn-Zn ferrite toroids.

occurs when the phase angle is zero. T36/23/10 shows the dimensional resonance at about 900 kHz.

B. Computational Models

The electric and magnetic fields in the measured samples are investigated by two different formulations. Due to the circumferential symmetry of the measurement setup [12], [13], the electromagnetic field distributions on any cross section along the circumference are the same. Consider a toroidal ferrite core with a rectangular cross section with outer radius R_2, inner radius R_1, and height d as depicted in Fig. 1 (right). Cylindrical coordinates r, φ, and z and frequency domain analysis are adopted. Assuming homogeneous and isotropic material, both the electric field strength ($\boldsymbol{E}$) and magnetic field strength ($\boldsymbol{H}$) are only functions of the radius r and independent of φ and z: $\boldsymbol{E} = E(r)\hat{z}$ and $\boldsymbol{H} = H(r)\ \hat{\varphi}$, where $\hat{z}$ and $\hat{\varphi}$ are the unit vectors in the z and φ directions, respectively. Therefore, the computational models are based on solving the Maxwell equations in the core in a 1-D axisymmetric setting. Small-signal variation is assumed, so that μ_{core} and ε_{core} can be assumed to be independent of the fields. From the Maxwell equations, the governing equations for the electromagnetic fields can be derived in terms of either $\boldsymbol{E}$ or $\boldsymbol{H}$. The formulations for both the $\boldsymbol{E}$- and $\boldsymbol{H}$-based models are written as

$$\begin{aligned} \nabla \times ((j\omega\mu)^{-1}\nabla \times \boldsymbol{E}) + (\sigma + j\omega\varepsilon)\boldsymbol{E} = 0, \\ \nabla \times ((\sigma + j\omega\varepsilon)^{-1}\nabla \times \boldsymbol{H}) + (j\omega\mu)\boldsymbol{H} = 0, \end{aligned} \tag{1}$$

where $\omega = 2\pi f$ is the angular frequency and σ is the conductivity which is obtained by DC measurement. The $\boldsymbol{E}$-based model is supplied by the measured voltage U and the $\boldsymbol{H}$-based model by the measured current I. The boundary conditions are written as

$$\begin{aligned} \frac{d\boldsymbol{E}}{dr}(r') = \boldsymbol{0},\ \boldsymbol{E}(R_2) = \frac{U}{d}\hat{z} \\ \boldsymbol{H}(r') = \boldsymbol{0},\ \boldsymbol{H}(R_2) = \frac{I}{2\pi R_2}\hat{\varphi} \end{aligned} \tag{2}$$

where r' denotes the left boundary of the model and can be set to $r' = R_1$ to model only the core or to $r' = 0$ to account also for the air at the center of the core.

Let $\Lambda(\omega) = [\mu_{core}, \varepsilon_{core}]$ be a vector which contains the unknown material parameters. The impedance $Z_c(\omega, \Lambda)$ can

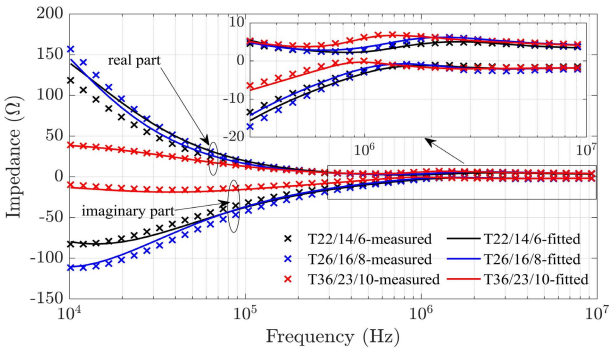

Fig. 3. Measured and fitted impedances for the Mn-Zn ferrite toroids.

be calculated by

$$Z_c = \frac{|U|^2}{\int\left((\sigma + j\omega\varepsilon)\|\boldsymbol{E}\|^2 + (j\omega\mu)^{-1}\|\nabla \times \boldsymbol{E}\|^2\right)d\Omega}, \\ = \frac{\int\left((\sigma + j\omega\varepsilon)^{-1}\|\nabla \times \boldsymbol{H}\|^2 + j\omega\mu\|\boldsymbol{H}\|^2\right)d\Omega}{|I|^2}, \quad (3)$$

where $\Omega = \Omega_{\text{core}}$ when only the core is modeled or $\Omega = \Omega_{\text{air}} \cup \Omega_{\text{core}}$ when also the air is considered. Standard Galerkin 1-D FEM is used for solving (1)–(3).

For extracting the dimension-independent material parameters μ_{core} and $\varepsilon_{\text{core}}$, we formulate the inverse problem as an optimization problem

$$\Lambda(\omega_i) = \text{argmin}_\Lambda |Z(\omega_i) - Z_c(\omega_i, \Lambda)|^2. \quad (4)$$

The FE models are combined with a non-linear least-squares algorithm for solving (4) and fitting μ_{core} and $\varepsilon_{\text{core}}$ at each frequency ω_i so that the calculated impedances match with the measured values [14].

III. Results

The $\boldsymbol{E}$- or $\boldsymbol{H}$-based model presented in Section II can be combined with the impedance measurements of the three toroidal cores for extracting the dimension-independent material parameters. It was observed that considering the air at the center of the core has negligible effect on the results in both models, which implies that it is enough to consider only the core with boundary conditions (2) at $r' = R_1$. The measured and fitted impedances of the toroidal cores used for extracting the dimension-independent μ_{core} and $\varepsilon_{\text{core}}$ are shown in Fig. 3. The dimension-independent μ_{core} is traced in the frequency range of 250 kHz–10 MHz, and it is comparable to the values provided in the datasheet as shown in Fig. 4 [9]. The permeability could not be traced below 250 kHz since it has negligible effect on the field solution at lower frequencies. The dimension-independent $\varepsilon_{\text{core}}$ is traced in the frequency range of 10 kHz–10 MHz as shown in Fig. 5. ε_r'' becomes negative around 1 MHz. There is no physical explanation for the negative values, and this failure might be attributed to a few reasons, i.e., the samples do not have identical material properties, the sensitivity of the inverse solver to the measurement data, and the noise level.

The distributions of the $\boldsymbol{E}$- and $\boldsymbol{H}$-fields along the radial position for T22/14/6 in the case that the air is considered at 432 kHz are shown in Fig. 6. It can be seen that the Neumann and Dirichlet conditions (2) for the $\boldsymbol{E}$- and $\boldsymbol{H}$-based models at $r' = R_1$ are reasonable when only the core is modeled. Moreover, the extracted parameters shown in Figs. 4 and 5

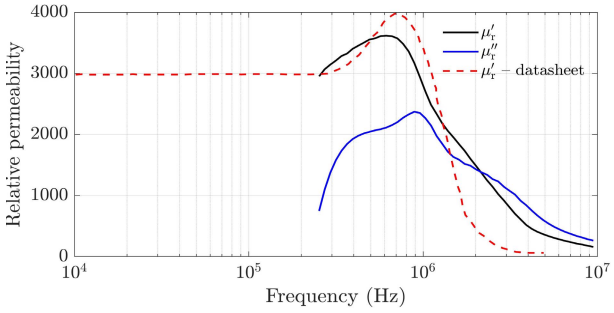

Fig. 4. Extracted dimension-independent relative complex permeability.

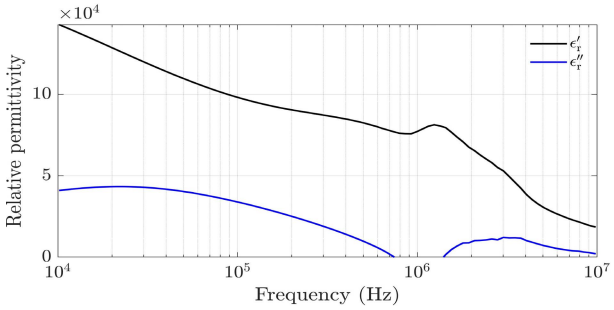

Fig. 5. Extracted dimension-independent relative complex permittivity.

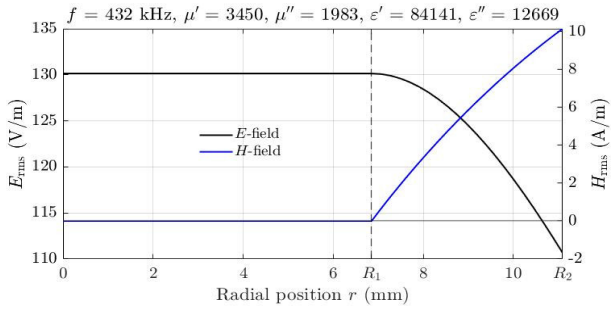

Fig. 6. Distributions of the root-mean-squared $\boldsymbol{E}$- and $\boldsymbol{H}$-fields along the radial position for T22/14/6.

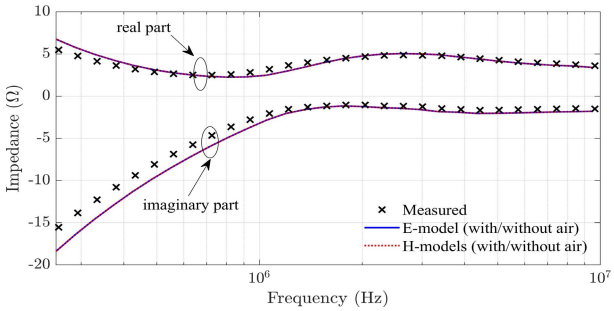

Fig. 7. FE simulations for T22/14/6 using the $\boldsymbol{E}$- and $\boldsymbol{H}$-based models with and without considering the air at the center of the core.

were used with the $\boldsymbol{E}$- and $\boldsymbol{H}$-based models to simulate the impedance of T22/14/6 in both cases, with and without considering the air at the center of the core. It is shown in Fig. 7 that the impedances calculated with the $\boldsymbol{E}$- and $\boldsymbol{H}$-based models match in both cases.

IV. Discussion and Conclusion

The $\boldsymbol{E}$- and $\boldsymbol{H}$-based formulations are presented in this work to solve the full-wave electromagnetic field equations in a toroidal ferrite core. The air at the center of the core has negligible effect on the field distributions in the core. The complex permeability cannot be traced well at low frequencies since the permeability does not have a significant effect on the field distribution. The extracted permeability agrees with the datasheet of the measured samples. The complex permittivity is traced for the whole frequency range, but the imaginary part has unreasonable negative values around 1 MHz.

Acknowledgment

This project has received funding from the European Research Council (ERC) under the European Union's Horizon 2020 research and innovation programme (grant agreement No 848590). Academy of Finland is acknowledged for financial support. Reda Elkhadrawy would like to thank Dr. Alexandre Halbach for the valuable discussions.

References

[1] Y. Sakaki, M. Yoshida, and T. Sato, "Formula for dynamic power loss in ferrite cores taking into account displacement current," *IEEE Trans. Magn.*, vol. 29, no. 6, pp. 3517–3519, Nov. 1993.

[2] J. Zhu, C. F. Foo, and P. Hing, "Dielectric loss analysis of toroid MnZn ferrite core," *Electron. Lett.*, vol. 35, no. 20, pp. 1746–1748, Sep. 1999.

[3] S. Lin, T. Brinker, L. Fauth, and J. Friebe, "Review of dimensional resonance effect for high frequency magnetic components," in *Proc. 21st Eur. Conf. Power Electron. Appl. (EPE ECCE Eur.)*, Genova, Italy, Sep. 2019, p. 1.

[4] D. Zhang and C. F. Foo, "A practical method to determine intrinsic complex permeabilities and permittivities for Mn-Zn ferrites," *IEEE Trans. Magn.*, vol. 41, no. 4, pp. 1226–1232, Apr. 2005.

[5] R. Huang and D. Zhang, "Experimentally verified Mn–Zn ferrites' intrinsic complex permittivity and permeability tracing technique using two ferrite capacitors," *IEEE Trans. Magn.*, vol. 43, no. 3, pp. 974–981, Mar. 2007.

[6] R. Huang and D. Zhang, "Using a single toroidal sample to determine the intrinsic complex permeability and permittivity of Mn–Zn ferrites," *IEEE Trans. Magn.*, vol. 43, no. 10, pp. 3807–3815, Oct. 2007.

[7] A. Stadler, M. Albach, and A. Lindner, "A practical method to measure electrical AC conductivity of MnZn ferrites using conventional toroids," *IEEE Trans. Magn.*, vol. 46, no. 2, pp. 678–681, Feb. 2010.

[8] *Alpha-A Modular Dielectric/Impedance Measurement System Mainframes*. Accessed: Feb. 2022. [Online]. Available: https://www.novocontrol.de/php/ana_alpha_main.php

[9] *F-Material Ferrites*. Accessed: Feb. 2022. [Online]. Available: https://www.mag-Inc.com/Products/Ferrite-Cores/F-Material

[10] T. P. Todorova, V. C. Valchev, and A. V. den Bossche, "Modelling of electrical properties of Mn-Zn ferrites taking into account the frequency of the occurrence of the dimensional resonance," *J. Electr. Eng.*, vol. 69, no. 3, pp. 219–225, Jul. 2018.

[11] M. Kacki, M. S. Rylko, J. G. Hayes, and C. R. Sullivan, "A practical method to define high frequency electrical properties of MnZn ferrites," in *Proc. IEEE Appl. Power Electron. Conf. Expo. (APEC)*, New Orleans, LO, USA, Mar. 2020, pp. 216–222.

[12] K. V. Namjoshi, J. D. Lavers, and P. P. Biringer, "Eddy-current power loss in toroidal cores with rectangular cross section," *IEEE Trans. Magn.*, vol. 34, no. 3, pp. 636–641, May 1998.

[13] A. Stadler, M. Albach, and A. Bucher, "Calculation of core losses in toroids with rectangular cross section," in *Proc. 12th Int. Power Electron. Motion Control Conf.*, Portoroz, Slovenia, Aug. 2006, pp. 828–833.

[14] J. Mueller and S. Siltanen, *Linear and Nonlinear Inverse Problems With Practical Applications* (Computational Science & Engineering), vol. 10. Philadelphia, PA, USA: SIAM, 2012.